Excited State Intramolecular Proton Transfer and Metal Ion Complexation of 2-(2′-Hydroxyphenyl)benzazoles in Aqueous Solution

Maged M. Henary and Christoph J. Fahrni*

School of Chemistry and Biochemistry, Georgia Institute of Technology, 770 State Street, Atlanta, Georgia 30332

Received: December 20, 2001; In Final Form: March 4, 2002

The excited-state intramolecular proton transfer (ESIPT) of a series of water-soluble 2-(2′-hydroxyphenyl)-benzazole derivatives has been studied under physiological conditions using absorbance and steady-state emission spectroscopy. At neutral pH in the presence of 0.1 M ionic background, the fluorescence properties of these derivatives differ substantially compared to previously reported data in nonaqueous solvents. The ESIPT process is disrupted, presumably due to intermolecular hydrogen bonding with surrounding water molecules combined with increased stabilization of the trans-rotamer, which cannot undergo the ESIPT process. The emission spectrum of the benzimidazole derivative depends significantly on the solvent polarity, as revealed by titrations with Zn(II) in methanol, ethanol, and under physiological conditions. Inhibition of ESIPT via metal coordination shows a significant wavelength shift together with a substantial ratio increase by a factor of 13.7. Titration of the benzoxazole derivative with Zn(II) yielded a 50-fold increased emission intensity. The fluorescence increase is specific for Zn(II), and with a log$K$ of 3.93 (K_d = 117 μM) the ligand would be suitable as a fluorescence probe in a biological environment to gauge Zn(II) concentrations in the range from 10 μM to 1 mM.

Introduction

Fluorescent sensor molecules for the detection of metal ions have attracted considerable research interest and led to the development of highly specific probes with a broad range of applications in environmental chemistry, biochemistry, and cell biology.[1] The majority of these chemosensors are based on a "switching on/off" mechanism, such that the fluorescent output is quenched in the absence, and restored upon binding of the analyte. Due to the linear relationship between fluorescence intensity and analyte concentration, such probes can principally be used for quantitative measurements. Since the emission intensity depends both on the analyte and the probe concentration, it is necessary to know the latter. This is in particular a limiting requirement for many biological applications since in a cellular environment, the dye concentration depends on many factors such as membrane permeability, incubation time and temperature, or variations in the cell size. Measured fluorescence intensities may vary significantly without actually reflecting differences in analyte concentrations. This problem can be solved using a fluorophore which displays a shift in the peak excitation or emission wavelength upon binding of the analyte. The ratio of the luminescence intensities at two excitation wavelengths is sufficient to determine the analyte concentration, independent of dye concentration or any instrument-related parameters.[2] Few such ratiometric probes have been developed for intracellular applications at present.[3] Due to the lack of suitable probes, the cell biology of many biologically important metal cations such as zinc, copper, manganese, and iron is still unexplored.

Molecules with intramolecular hydrogen bonds often exhibit photoinduced proton-transfer processes, a phenomenon which has widespread implications in the action of many laser dyes,[4,5] as high-energy radiation detectors,[6−8] UV photostabilizers,[9,10] and fluorescent probes.[11−13] In the case of the adiabatic, barrierless excited-state intramolecular proton transfer (ESIPT), a covalently attached proton, typically of a hydroxyl or amino group, in the electronically excited-state migrates to a neighboring hydrogen-bonded atom less than 2 Å away. The formed phototautomer emits light and thermally equilibrates back to the ground state with the proton bound to its original atom. This process can proceed extremely fast and several studies have found subpicosecond reaction rates for a variety of molecules, even in rigid media or at temperatures as low as 4 K.[14−21] Recent femtosecond transient spectroscopy measurements show that the proton takes 60 fs to arrive at its tautomer equilibrium position. The electron distribution changes on the same time scale, but the nuclear framework cannot adjust to the new structure as quickly and starts to strongly vibrate in low-frequency skeletal modes.[22−24] Since the formed phototautomer is only more stable in the excited state but not the ground state, the observed Stokes shift of the fluorescence emission is unusually large with values ranging from 100 to 500 nm.[25] Furthermore, ESIPT molecules often exhibit dual emission: besides the red-shifted tautomer emission, a normal emission at higher energy can be observed. The overall fluorescence emission spectrum depends on the nature of both the ground and excited state of the molecule and is often strongly influenced by the pH as well as the hydrogen-bonding ability and polarity of the solvent.[26,27] These properties render ESIPT molecules interesting targets for the development of ratiometric fluorescent probes.

In this study, we explore the influence of metal cation binding on the proton-transfer process. The chelation of metal cations often competes with protonation of the ligand donor atoms and therefore the emission of ESIPT molecules is expected to be responsive toward metal coordination. If the proton transfer

* To whom correspondence should be addressed. Phone: 404-385-1164/ fax: 404-894-2295. Email address: fahrni@chemistry.gatech.edu.

10.1021/jp014634j CCC: $22.00
Published on Web 05/08/2002

SCHEME 1

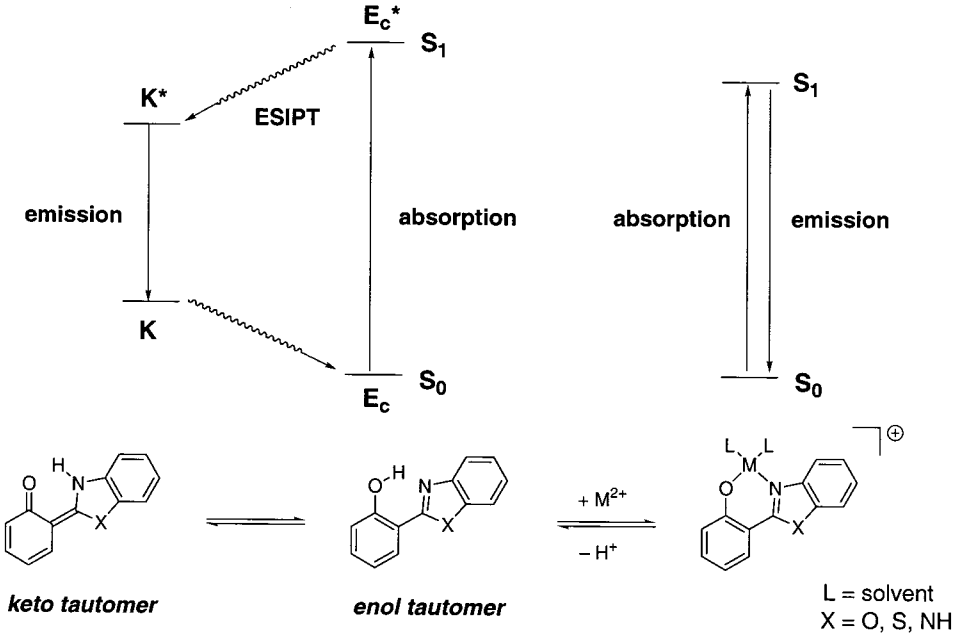

process is efficiently disrupted by the coordinated metal cation, the red-shifted tautomer emission is expected to disappear in favor of the normal emission of the metal-complex at higher energy. Fluorescent probes which are based on inhibition of ESIPT therefore have the potential to undergo large shifts of the peak emission energy. A shift of the peak excitation energy is generally preferred when monitoring the probe response in biological samples with a standard fluorescence microscope setup.[28] Commercially available ratiometric imaging systems offer up to millisecond time resolution using a high-speed excitation monochromator. Nevertheless, with the development of two-photon microscopy imaging, most of the popular ratiometric probes used in cell biology are not applicable.[29−31] These dyes often show only little shift in the peak emission and can only be used for ratiometric measurements at two excitation energies. Two-photon microscopy imaging requires an expensive pumped-laser system, which does not allow fast switching between two different excitation wavelengths. In contrast, the sample emission can be monitored at two different wavelengths with a rotating filter wheel without requiring expensive modifications of the instrument. Consequently, to benefit from the considerable advantages of two-photon microscopy, a new generation of ratiometric probes is required which exhibits large shifts of the emission energy upon binding of the analyte.

In recent years, the general family of 2-(2′-hydroxyphenyl)-benzazoles has been studied extensively to elucidate the mechanism of the excited-state intramolecular proton-transfer process.[21,32−44] The wealth of information available about the photophysics of benzazole derivatives prompted us to choose this class of molecules as an attractive starting point to explore the influence of cation binding on the proton-transfer process. The presence of an intramolecular hydrogen bond is vital to the ESIPT process. At the same time, the special properties of water with its high polarity and capacity to form hydrogen bonds might interfere and ESIPT processes that occur in nonpolar solvents cannot necessarily be extrapolated to water. Surprisingly, the enol form of 2-(2′-hydroxyphenyl)benzimidazole (HBI) undergoes ESIPT with almost 100% efficiency in nonpolar as well as protic solvents such as ethanol or neat water.[34] If coordination of a metal cation is accompanied by displacement of the hydroxyl proton, the ESIPT process is no longer possible and a substantial blue shift in the peak emission would be expected (Scheme 1).

Since our primary goal is to develop fluorescence probes for biological applications, we conducted our studies under physiological conditions in aqueous solution at neutral pH and limited the selection of cations to biologically important metals such as Ca(II), Mg(II), Zn(II), Fe(II), and Cu(II). Only heavy and transition metal ions, such as Zn(II), Cd(II), Cu(II), or Fe(II), bind with significant affinity to the 2-(2′-hydroxyphenyl)-benzazole ligands under physiological conditions. Among the biologically important metals, only Zn(II) ions form a fluorescent complex, whereas the complexes with paramagnetic transition metal ions are nonfluorescent. For this reason, the present work focuses primarily on the investigation of the Zn(II) complexes by means of absorption and steady-state emission spectroscopy. Due to the poor solubility of the benzazole ligands and their transition metal complexes in aqueous solution at neutral pH, the ligand framework was slightly modified by introduction of a carboxylic acid functionality (Scheme 2). Since carboxylic acids are fully dissociated at neutral pH, the solubility of the ligands in water is greatly enhanced. The acid functionality is spatially separated from the metal binding site and is not expected to interfere with the ESIPT process or metal coordination.

Experimental Section

Materials and Reagents. 2-Aminophenol (Aldrich, 99%), 2-amino-thiophenol (Aldrich, tech., 90%), *o*-phenylenediamine (Aldrich, 99%), barium manganate (Aldrich, tech., 90%), 1,4-benzoquinone (Aldrich, 98%), ferric chloride hexahydrate (Aldrich, 98%), (4-formyl-3-hydroxy-phenoxy)-acetic acid ethyl-ester (**1**) was synthesized following a literature procedure.[45] NMR: δ in ppm vs $SiMe_4$ (0 ppm, ^1H, 300 MHz). MS: selected peaks; *m*/*z*. Melting points are uncorrected. Flash chromatography (FC): Merck silica gel (70−230 mesh). TLC: 0.25 mm, Merck silica gel 60 F254, visualizing at 254 nm or with 2% $KMnO_4$ solution. Analytical experiments: Buffer solutions were made with ultrapure deionized water (18 Ω resistance). PIPES (Sigma-Aldrich, 99%), $Zn(OTf)_2$ (Aldrich), $Cu(NO_3)_2 \cdot 5H_2O$

SCHEME 2

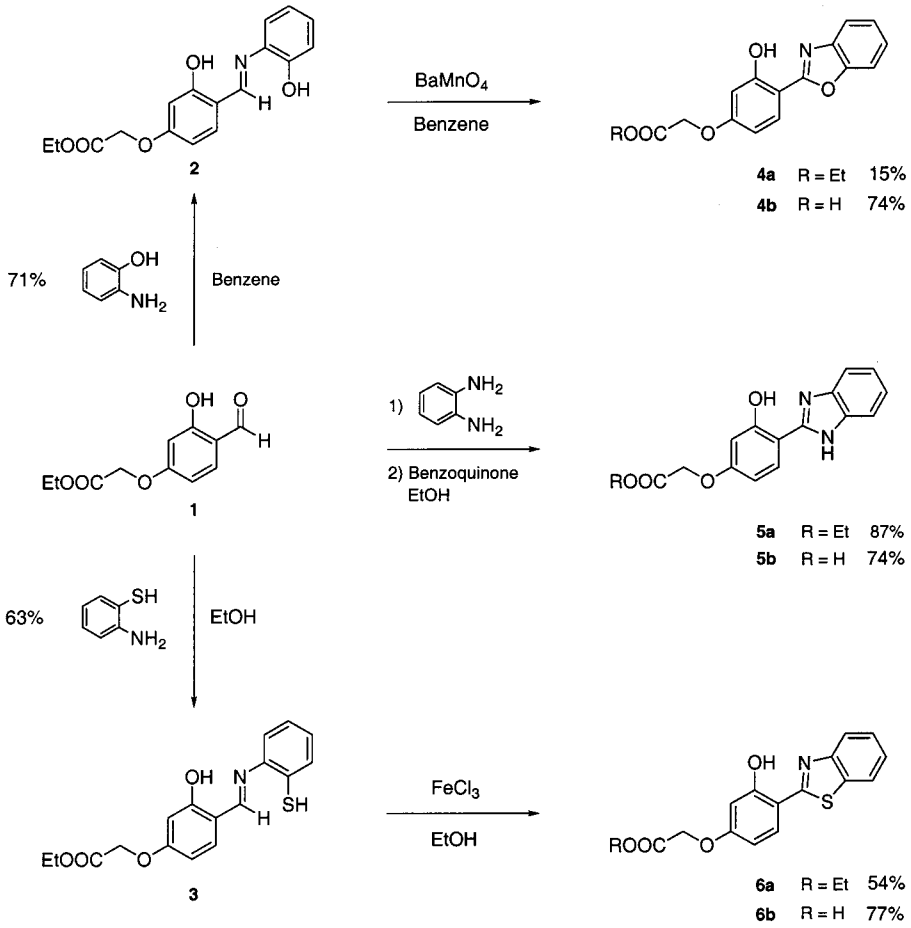

(Aldrich), $Fe(BF_4)_2 \cdot 6H_2O$ (Strem), $Ca(NO_3)_2 \cdot 4H_2O$ (Aldrich), $Mg(NO_3)_2 \cdot 6H_2O$, KNO_3 (Aldrich, 99%), KCl (Aldrich, 99%).

Synthesis. (a) {3-Hydroxy-4-[(2-hydroxy-phenylimino)-methyl]-phenoxy}-acetic acid ethyl ester (2). A solution of aldehyde **1** (250 mg, 1.12 mmol) and 2-amino-phenol (128 mg, 1.17 mmol) in benzene (15 mL) was heated under reflux using a Dean−Stark condenser for continuous removal of water. After 12 h the reaction mixture was cooled to room temperature and concentrated in vacuo. The yellow solid residue was recrystallized from ether providing 251 mg (0.79 mmol, 71%) of Schiff base **2** as yellow solid: mp 206−208 °C; R_f 0.25 (1:1 hexane: EtOAc); ^{1}H NMR (DMSO-d_6, 300 MHz) δ 1.22 (t, J = 7.1 Hz, 3H), 4.18 (q, J = 7.1 Hz, 2H), 4.83 (s, 2H), 6.36 (s, 1H), 6.48 (d, J = 8.8 Hz, 1H), 6.86 (t, J = 7.4 Hz, 1H), 6.94 (d, J = 8.2 Hz, 1H), 7.09 (t, J = 7.7 Hz, 1H), 7.35 (d, J = 7.7 Hz, 1H), 7.47 (d, J = 8.8 Hz, 1H), 8.86 (s, 1H), 9.80 (s, 1H), 14.38 (s, broad, 1H); MS (70 eV) 315 (M^+, 100), 314 (48), 120 (24), 43 (35). EI−HRMS *m*/*e* calculated for $C_{17}H_{17}NO_5$ 315.11067, found 315.11088.

(b) {3-Hydroxy-4-[(2-mercapto-phenylimino)-methyl]-phenoxy}-acetic acid ethyl ester (3). A solution of aldehyde **1** (208 mg, 0.93 mmol) and 2-aminothiophenol (116 mg, 0.93 mmol) in EtOH (8 mL) was heated under reflux for 12 h. The mixture was cooled to room temperature, concentrated in vacuo and the residue crystallized from ether yielding 193 mg (0.58 mmol, 63%) of Schiff base **3** as yellow solid: mp 129−130 °C; R_f 0.23 (1:1 hexane:EtOAc); ^{1}H NMR (DMSO-d_6, 300 MHz) δ 1.22 (t, J = 7.1 Hz, 3H), 4.19 (q, J = 7.1 Hz, 2H), 4.88 (s, 2H), 6.52 (s, 1H), 6.62 (d, J = 8.2 Hz, 1H), 7.26 (t, J = 7.1 Hz, 1H), 7.35 (t, J = 7.1 Hz, 1H), 7.48 (d, J = 7.7 Hz, 1H), 7.54 (d, J = 7.7 Hz, 1H), 7.62 (d, J = 8.8 Hz, 1H), 8.94 (s, 1H), 13.07 (s, broad, 1H).

(c) (4-Benzoxazol-2-yl-3-hydroxy-phenoxy)-acetic acid ethyl ester (4a). A mixture of imine **2** (215 mg, 0.68 mmol) and $BaMnO_4$ (700 mg, 2.73 mmol) in benzene (10 mL) was heated under reflux for 3 h. The mixture was cooled to room temperature and the residue filtered through Celite and concentrated in vacuo. The black residue was further purified on silica gel (FC, hexane-CH_2Cl_2, 3:1 → 1:1, to give 33 mg (0.11 mmol, 15%) of oxazole **4a** as colorless solid: mp 123−124 °C; R_f 0.38 (3:1 hexanes−EtOAc); ^{1}H NMR ($CDCl_3$, 300 MHz) δ 1.32 (t, J = 7.1 Hz, 3H), 4.30 (q, J = 7.1, 2H), 4.68 (s, 2H), 6.59−6.65 (m, 2H), 7.32−7.39 (m, 2H), 7.55−7.60 (m, 1H), 7.66−7.72 (m, 1H), 7.95 (d, J = 8.8 Hz, 1H), 11.65 (s, 1H); MS (70 eV) 313 (M^+, 100), 210 (32), 182 (22), 36 (18). EI−HRMS *m*/*e* calculated for $C_{17}H_{15}NO_5$ 313.09502, found 313.09747.

(d) (4-Benzoxazol-2-yl-3-hydroxy-phenoxy)-acetic acid (4b). To a solution of $LiOH \cdot H_2O$ (97 mg) in a mixture of H_2O (1.5 mL), THF (2 mL), and MeOH (1.5 mL) was added **4a** (55 mg, 0.18 mmol). The reaction mixture was heated under reflux for 2.5 h, cooled to room temperature, and the organic solvents were removed in vacuo. The mixture was diluted with H_2O (2 mL) and the product precipitated by dropwise addition of aq. HCl (1 M). The product was filtered off, washed with little H_2O, and dried in vacuo affording 37 mg (0.13 mmol, 74%) of acid **4b** as colorless solid. mp 232−234 °C; ^{1}H NMR (DMSO-d_6, 300 MHz) δ 4.77 (s, 2H), 6.62−6.68 (m, 2H), 7.38−7.45 (m, 2H), 7.75−7.82 (m, 2H), 7.92 (d, J = 8.8 Hz, 1H), 11.35 (s, 1H), 13.10 (s, broad, 1H); MS (70 eV) 285 (M^+, 100), 227

(18), 198 (38). EI−HRMS *m*/*e* calculated for $C_{15}H_{11}NO_5$ 285.06372, found 285.05910.

(e) [4-(1H−Benzimidazol-2-yl)-3-hydroxy-phenoxy)]-acetic acid ethyl ester (5a). A solution of aldehyde **1** (200 mg, 0.89 mmol) and *o*-phenylenediamine (96 mg, 0.89 mmol) in EtOH (10 mL) was heated under reflux for 2 h. After addition of 1,4-benzoquinone (192 mg, 1.78 mmol) the mixture was further refluxed for 0.5 h. The reaction mixture was cooled to room temperature, and quenched by dropwise addition of saturated aq. $NaHCO_3$ (20 mL). The mixture was extracted with EtOAc (2 × 20 mL) and the combined organic layers were washed with H_2O (2 × 10 mL), dried ($MgSO_4$), and concentrated in vacuo. The residue was further purified on silica gel (FC, hexanes−EtOAc, 4:1 → 2:1, yielding 245 mg (0.78 mmol, 87%) of imidazole **5a** as colorless solid. mp 194−196 °C; R_f 0.36 (2:1 hexane:EtOAc); ^{1}H NMR ($CDCl_3$, 300 MHz) δ 1.23 (t, J = 7.1 Hz, 3H), 4.20 (q, J = 7.1 Hz, 2H), 4.85 (s, 2H), 6.57 (d, J = 2.5 Hz, 1H), 6.65 (dd, J = 8.8, 2.5 Hz, 1H), 7.22−7.28 (m, 2H), 7.62 (s, broad, 2H), 7.95 (d, J = 8.8 Hz, 1H), 13.0 (s, broad, 1H), 13.4 (b, broad, 1H); MS (70 eV) 312 (M^+, 100), 197 (30). EI−HRMS *m*/*e* calculated for $C_{17}H_{16}N_2O_4$ 312.11101, found 312.11186.

(f) [4-(1H−Benzimidazol-2-yl)-3-hydroxy-phenoxy)]-acetic acid (5b). Ester **5a** (200 mg, 0.64 mmol) was hydrolyzed following the procedure as described for ester **4a** yielding 135 mg (0.47 mmol, 74%) of acid **5b** as tan solid. mp > 300 °C; ^{1}H NMR (DMSO-d_6, 300 MHz) δ 4.75 (s, 2H), 6.55 (d, J = 2.2 Hz, 1H), 6.64 (dd, J = 8.8, 2.2 Hz, 1H), 7.27 (dd, J = 6.0, 3.0 Hz, 2H), 7.63 (dd, J = 6.0, 3.1 Hz, 2H), 7.99 (d, J = 8.8 Hz, 1H), 13.18 (s, broad, 3H); MS (70 eV) 284 (M^+, 100), 197 (61), 36 (23). EI−HRMS *m*/*e* calculated for $C_{15}H_{12}N_2O_4$ 284.07971, found 284.07969.

(g) (4-Benzothiazol-2-yl-3-hydroxy-phenoxy)-acetic acid ethyl ester (6a). To a hot solution of $FeCl_3 \cdot 6\ H_2O$ (462 mg, 1.71 mmol) in EtOH (5 mL) a solution of imine **3** (142 mg, 0.43 mmol) in EtOH (2 mL) was added, and the resulting mixture was heated under reflux for 0.5 h. The dark mixture was cooled to room temperature, diluted with H_2O (3 mL) and extracted with EtOAc (2 × 10 mL). The combined organic extracts were dried ($MgSO_4$) and concentrated in vacuo affording a brown residue, which was further purified on silica gel (FC, hexanes−EtOAc, 5:1 → 3:1, providing 76 mg (0.23 mmol, 54%) of benzothiazole **6a** as pale greenish solid mp 137−139 °C; R_f 0.38 (3:1 hexane:EtOAc); ^{1}H NMR ($CDCl_3$, 300 MHz) δ 1.32 (t, J = 7.1 Hz, 3H), 4.30 (q, J = 7.1 Hz, 2H), 4.67 (s, 2H), 6.55−6.62 (m, 2H), 7.38 (t, J = 7.1 Hz, 1H), 7.49 (t, J = 8.2 Hz, 1H), 7.60 (d, J = 8.8 Hz, 1H), 7.87 (d, J = 8.8 Hz, 1H), 7.94 (d, J = 8.2 Hz, 1H), 12.71 (s, broad, 1H); MS (70 eV) 329 (M^+, 100), 256 (20), 226 (38), 214 (43), 198 (31). EI−HRMS *m*/*e* calculated for $C_{17}H_{15}NO_4S$ 329.07218, found 329.07211.

(h) (4-Benzothiazol-2-yl-3-hydroxy-phenoxy)-acetic acid (6b). Ester **6a** (44 mg, 0.13 mmol) was hydrolyzed following the procedure as described for ester **4a** affording 31 mg (0.103 mmol, 77%) of acid **6b** as pale tan solid: mp 226−228 °C; ^{1}H NMR (DMSO-d_6, 300 MHz) δ 4.75 (s, 2H), 6.57 (d, J = 2.8 Hz, 1H), 6.62 (dd, J = 11.1, 2.6 Hz, 1H), 7.40 (td, J = 8.7 Hz, 1.6 Hz, 1H), 7.52 (td, J = 8.7 Hz, 1.6 Hz, 1H), 7.98−8.10 (m, 3H), 11.81 (s, broad, 1H), 13.12 (s, broad, 1H); MS (70 eV) 301 (M^+, 100), 214 (45), 186 (18). EI−HRMS *m*/*e* calculated for $C_{15}H_{11}NO_4S$ 301.04088, found 301.04140.

Steady-State Absorption and Fluorescence Spectroscopy. All sample stock solutions and buffer solutions were filtered through 0.2-μm nylon membrane filters to remove interfering dust particles or fibers. UV−vis absorption spectra were recorded at 25 °C using a Varian Cary Bio50 UV−vis spectrometer with constant-temperature accessory. Steady-state emission and excitation spectra were recorded with a PTI fluorimeter and FELIX software. Throughout the titration the sample solution was stirred with a magnetic stirring device. For all titrations the path length was 1 cm with a cell volume of 3.0 mL. All fluorescence spectra have been corrected for the spectral response of the detection system (emission correction file provided by instrument manufacturer) and for the spectral irradiance of the excitation channel (via calibrated photodiode). Quantum yields were determined using quinine sulfate dihydrate in 1.0 N H_2SO_4 ($\Phi_f = 0.54 \pm 0.05$) as fluorescence standard.[46]

Electrode Calibration in Aqueous Solution. Measurements were performed with a Mettler Inlab combination glass electrode (Model No. 423). For the determination of the pK values in aqueous solution, the electrode was calibrated for -log[H_3O^+] by titration of a standardized HCl solution (Aldrich, 0.1 N volumetric standard) with KOH (Aldrich, 0.1 N volumetric standard) at 25 °C and 0.1 M ionic strength (KCl). The end point, $E°$, and slope were determined using Gran's method[47] as implemented in the software GLEE.[48] The calibration procedure was repeated three times prior to each pK value determination. The electrode potential was measured with the Corning pH/Ion Analyzer 355 and the emf measurements were reproducible with ±0.1 mV accuracy. For the determination of the apparent stability constants, the electrode was calibrated using commercial pH reference solutions.

Determination of pK Values. All protonation constants reported in this study were determined from absorption measurements. The UV−vis absorption spectra of the ligands were monitored for a series of solution in which -log[H_3O^+] was varied between 5 and 11. The emf of each solution was directly measured in the UV quartz cell (electrode diameter 3 mm) and converted to -log[H_3O^+] using $E°$ and slope as obtained from the electrode calibration procedure described above. The raw spectral and emf data were processed via nonlinear least-squares fit analysis using the SPECFIT software package.[49]

Complex Stability Constants. All measured cation stability constants K, reported herein, were measured at pH 7.2 (PIPES 10 mM, 0.1 M KNO_3 ionic strength) and are therefore apparent stability constants. To 3.0 mL of a 30 μM solution of the corresponding ligand in PIPES buffer (10 mM, pH 7.20, 0.1 M KNO_3) were added 5 μL aliquots of $Zn(OTf)_2$ stock solution (concentration 5 mM, 50 mM or 0.5 M). Upon each addition the solution was stirred for 15 min to reach equilibrium and the UV−vis spectrum was subsequently monitored. The recorded UV−vis traces were analyzed by a nonlinear least-squares fit algorithm using an equilibrium model with 1:1 complex stoichiometry (SPECFIT software).[49]

Results and Discussion

Synthesis. The preparation of all three benzazole derivatives **4**−**6** is based on the salicylic aldehyde precursor **1** which was synthesized according to a published procedure (Scheme 2).[45] The benzoxazole derivative **4a** was obtained by condensation of **1** with 2-aminophenol to give the Schiff base **2**. Initial attempts to cyclize and oxidize **2** with Fe(III) chloride resulted in hydrolysis of the imino group, and aldehyde **1** was the only observed product. In contrast, treatment with barium manganate gave the desired oxazole **4a**, but only with low yield. The low yield is presumably due to decomposition, since no other products could be isolated. Benzimidazole **5a** was synthesized via condensation of **1** with *o*-phenylenediamine followed by oxidation of the dihydroimidazole intermediate with

TABLE 1: Protonation Constants and Photophysical Data of Benzazole 4b, 5b, and 6b in Aqueous Solution[a]

species	data	oxazole (**4b**)	imidazole (**5b**)	thiazole (**6b**)
pK_1	$[LH^-]/[L^{2-}][H^+]$	9.28 ± 0.01	8.63 ± 0.01	8.25 ± 0.01
pK_2	$[LH_2]/[LH^-][H^+]$	n.a.	5.90 ± 0.01	n.a.
L^{2-}	Absorption[b] λ_{max} (nm), $\epsilon(cm^{-1}M^{-1})$	347, 18500	340, 22200	369, 16300
	Excitation[c] λ_{max} (nm)	347 (420)[e]	341 (396)[e]	370 (448)[e]
	Emission[c] λ_{max} (nm)	420 (350)[f]	396 (350)[f]	448 (350)[f]
	Quantum Yield[e]	0.29	0.63	0.79
	Stokes Shift (cm^{-1})	5008	4159	4778
LH^-	Absorption[b] λ_{max} (nm), $\epsilon(cm^{-1}M^{-1})$	317, 29400	316, 22400	323, 19900
	Excitation[d] λ_{max} (nm)	329 (417)[e], 326 (364)[e]	332 (355)[e]	340 (436)[e]
	Emission[d] λ_{max} (nm)	364 (320)[f], 417 (350)[f]	355 (332)[f], 424 (372)[f]	436 (340)[f]
	Stokes Shift (cm^{-1})	4073, 7564	3476, 8060	8023
	Quantum Yield	0.07	0.25	0.05
LH_2	Absorption[b] λ_{max} (nm), $\epsilon(cm^{-1}M^{-1})$	n.a.	325, 28100	n.a.

[a] 0.1 M KNO_3, 25 °C. [b] Deconvoluted spectra from pH titration. [c] pH 11.20, 0.1M KNO_3. [d] pH 7.20, 10 mM PIPES. [e] Emission wavelength in parentheses. [f] Excitation wavelength in parentheses.

1,4-benzoquinone to afford **5a** in 87% yield. Hydroquinone which was formed as a byproduct from the reduction of 1,4-benzoquinone could be easily separated by extraction with aqueous bicarbonate solution. Altogether, the one-pot procedure provides access to gram quantities of the benzimidazole derivative under mild conditions and with high yield. Finally, condensation of **1** with 2-aminothiophenol gave imine **3** with 63% yield. In contrast to the benzoxazole derivative **4**, cyclization and oxidation by Fe(III) chloride were successful and provided the corresponding benzothiazole derivative **6a** with 54% yield. All analytical studies were carried out with the acids **4b**, **5b**, and **6b**, which were obtained by hydrolysis of the corresponding esters with lithium hydroxide in a methanol-THF-water solvent mixture.

Most previously published procedures for the synthesis of benzazoles are based on carboxylic acids, acid chlorides, or esters as the condensation partner and require much harsher reaction conditions (e.g. polyphosphoric acid at 250 °C or nitrobenzene at 150 °C),[50] which are not compatible with the ester functionality. The outlined synthesis gives access to benzazoles under mild conditions and should be suitable for the synthesis of a broad range of functionalized benzazoles.

Protonation Equilibria

Absorption Spectra. The pK values for the three benzazole ligands **4b**, **5b**, and **6b** were measured by spectrophotometric titrations. The UV absorption spectra were monitored for solutions in which -log[H_3O^+] was varied between 5 and 11 while keeping the ionic strength constant with 0.1 M KNO_3. At higher H_3O^+ concentrations (-log[H_3O^+] < 5), the ligand started to precipitate and therefore the pK values of the carboxylic acid moiety could not be determined by this method. The UV−vis traces were analyzed over the entire wavelength range using a nonlinear least-squares fit algorithm as implemented in the SPECFIT software package.[49,51] The fitting procedure not only yielded the protonation constants, but also allowed spectral deconvolution to determine the UV spectra for all involved species (Figure 1). A compilation of the curve fitting results including photophysical properties of the individual species is given in Table 1. Both the oxazole **4b** and thiazole **6b** gave UV traces with a single set of isosbestic points within the studied -log[H_3O^+] range, suggesting the presence of a single protonation equilibrium. The pK value can be assigned to protonation of the phenolic oxygen which is consistent with the observed red-shifted maximum in the spectrum of the fully deprotonated ligand (L^{2-}). The proton affinity of the thiazole ligand was found to be substantially lower (8.25) as compared

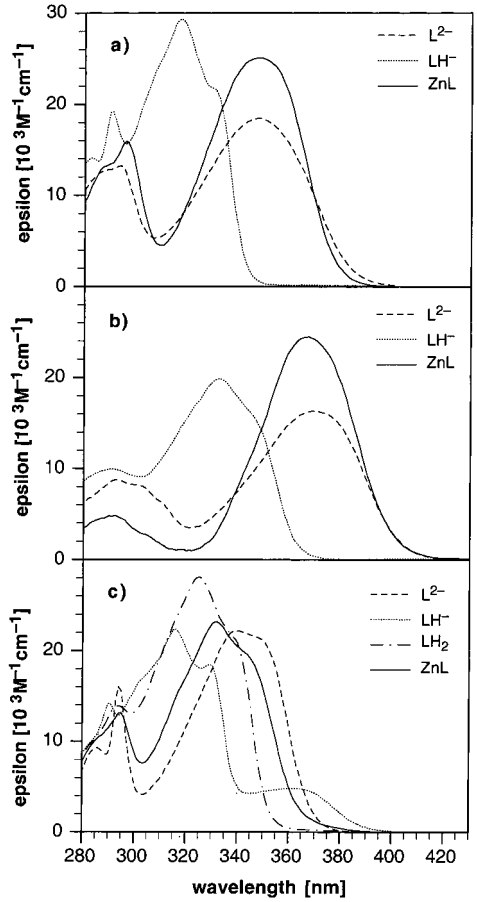

Figure 1. Deconvoluted UV−vis absorbance spectra for a) oxazole **4b**, b) thiazole **6b** and c) imidazole **5b**. The spectra for the fully deprotonated (L^{2-}) and monoprotonated (LH^-) ligand (0.1 M KNO_3, 25 °C) were obtained from pH titrations (In case of ligand **5b** a double-protonated species (LH_2) was detected). The plotted UV−vis traces for the 1:1 zinc(II)-ligand complex (ZnL) were obtained from the corresponding spectrophotometric Zn(II) titrations at constant pH 7.20 via deconvolution (10 mM PIPES, 0.1 M KNO_3, 25 °C).

to the oxazole derivative (9.28), which is consistent with the differences in pi-donor and sigma-acceptor properties of sulfur and oxygen. A similar trend was reported for the unsubstituted 2-(2′-hydroxyphenyl)-benzothiazole and -benzoxazole derivatives in mixed aqueous−organic solvent. Under these conditions the pK values also differ by approximately one order of magnitude.[52] In contrast, the UV-titration of the benzimidazole derivative **5b** shows two distinct regions, each containing a characteristic set of isosbestic points (Figure 2a), which suggests

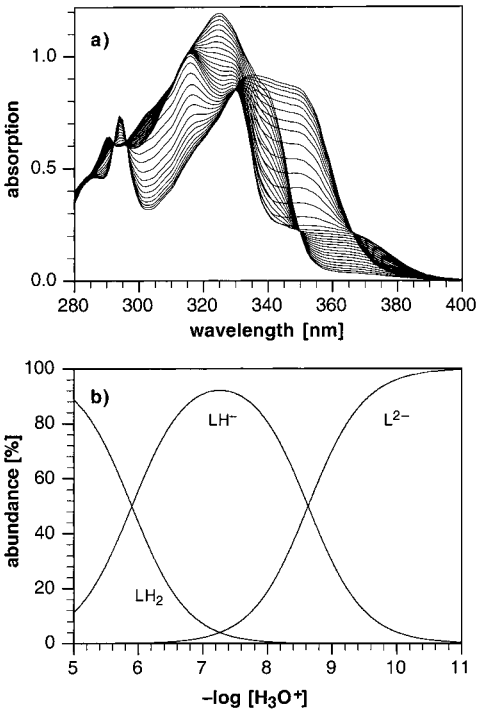

Figure 2. a) UV−vis absorbance of ligand **5b** as a function of pH (-log[H_3O^+] ranging between 5 and 11, μ = 0.1 M KNO_3, 25 °C). b) Calculated species distribution diagram as a function of -log[H_3O^+].

SCHEME 3

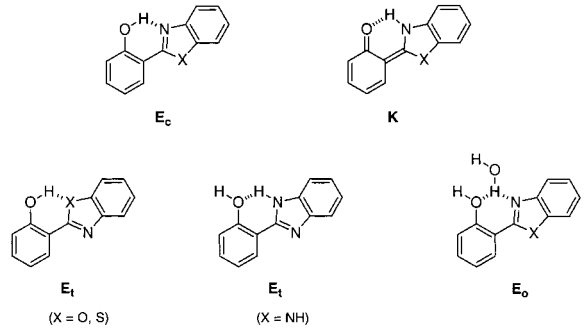

the presence of an additional protonation equilibrium in the analyzed pH range. The first p*K* value was found to be 8.63 and lies between the p*K* of the thiazole and oxazole ligands, and the absorption maximum of the fully deprotonated phenolate anion (L^{2-}) is also red-shifted compared to the mono- (LH^-) and diprotonated (LH_2) species (Figure 1c). The second p*K* value of 5.90 is too high for protonation of the carboxylic acid, but within the expected range for protonation of the benzimidazole nitrogen (p*K* of benzimidazole = 5.68).[53] Furthermore, the deconvoluted UV spectrum of the monoprotonated ligand (LH^-) shows an additional absorption band at lower energy (360 nm), which was not observed for the oxazole nor the thiazole ligand. This absorption band has been previously assigned to the keto tautomer **K** (Scheme 3), which is in equilibrium with the enol form at neutral pH.[34] The absence of the lower energy absorption band in the spectra of the benzoxazole and thiazole ligands suggests that the keto tautomer does not contribute to the ground-state equilibrium of these derivatives. Based on the measured p*K* values, a species distribution plot was calculated for benzimidazole ligand **5b** (Figure 2b). At neutral pH the monoprotonated ligand shows an abundance of more than 90% and is therefore the major species present in the equilibrium. The benzazole nitrogen atom of the oxazole and thiazol

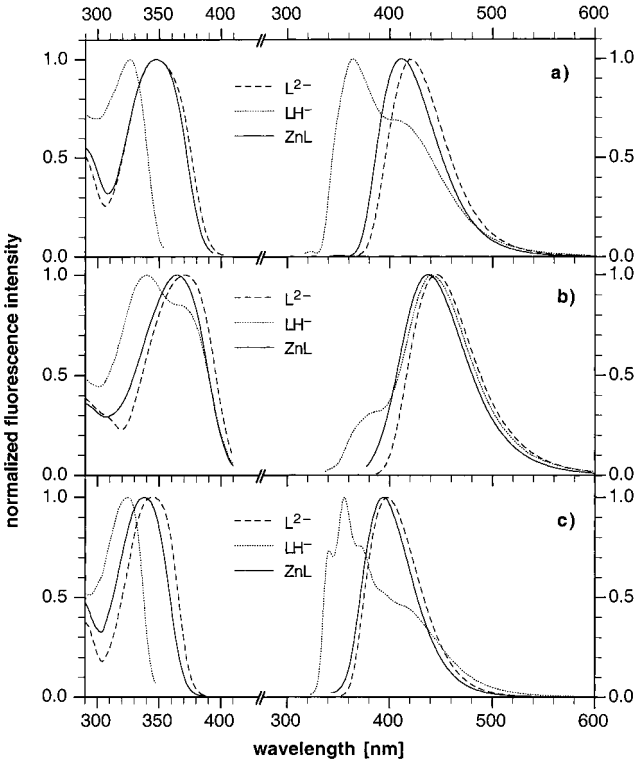

Figure 3. Normalized fluorescence emission and excitation spectra for a) oxazole **4b**, b) thiazole **6b** and c) imidazole **5b** in aqueous solution. All spectra were monitored with 0.1 M KNO_3 ionic background at 25 °C. The traces for the monoprotonated ligand (LH^-) were measured at pH 7.20 (10 mM PIPES), the spectra of the fully deprotonated ligand (L^{2-}) were acquired at pH 11.2 (unbuffered). The spectra of the Zn(II) complex were recorded at 5 mM total $Zn(OTf)_2$ for (a) and (c) and 500 mM $Zn(OTf)_2$ for graph (b).

derivatives **4b** and **6b** is considerably less basic, and only a single protonation equilibrium was observed for -log[H_3O^+] between 5 and 11. Conclusively, under neutral conditions the monoprotonated ligand is the predominant species for both derivatives.

Fluorescence Spectra. The excitation and emission spectra for the three benzazole ligands were recorded at pH 7.2 and 11.2 in buffered aqueous solution (Figure 3). Several previous studies of unsubstituted 2-(2′-hydroxyphenyl)-benzazole were performed in ethanol.[32−34,36] To allow a direct comparison with these literature data, we also measured the photophysical properties of the ester derivatives **4a**, **5a**, and **6a** in neat ethanol and in basic ethanolic solution (Figure 4). A compilation of all photophysical properties is given in Tables 1 and 2.

In aqueous solution at neutral pH, the emission spectrum of the oxazole ligand **4b** exhibits two maxima at 364 and 417 nm, respectively, with a low quantum yield of 3% (Figure 3a). Possible mechanisms accounting for the nonradiative loss of energy include solute−solvent interactions, torsional motions of the two rings, or triplet population.[37,54,55] In ethanol, the higher energy emission band was observed at approximately the same wavelength (360 nm), whereas the second, lower energy emission is considerably red-shifted to 464 nm (Figure 4a). Previous studies have shown that the intensity of the normal emission at shorter wavelength is strongly solvent dependent and generally very weak in a nonpolar environment.[33] The emission has been assigned to the trans-rotamer E_t, which cannot undergo excited-state intramolecular proton transfer (Scheme 3). The excitation spectra corresponding to the two emission bands differ substantially, both in ethanol and aqueous solution,

TABLE 2: Photophysical Data of Benzazole 4a, 5a, and 6a in Ethanol at 25 °C

species	data	oxazole (**4a**)	imidazole (**5a**)	thiazole (**6a**)
L^-	Absorption[a] λ_{max} (nm), ϵ($cm^{-1}M^{-1}$)	341, 17900	356, 17400	380, 22800
	Excitation[a] λ_{max} (nm)	349 (420)[c]	339 (393)[c]	366 (444)[c]
	Emission[a] λ_{max} (nm)	420 (349)[d]	393 (339)[d]	444 (366)[d]
	Stokes Shift (cm^{-1})	5515	2644	3793
LH	Absorption[b] λ_{max} (nm), ϵ($cm^{-1}M^{-1}$)	318, 23600	319, 26400	335, 26600
	Excitation[b] λ_{max} (nm)	300 (360)[c]	314 (435)[c]	320 (375)[c]
	Emission[b] λ_{max} (nm)	360, 464 (300)[d]	435 (314)[d]	375 (320)[d]
	Stokes Shift (cm^{-1})	3668, 9895	8359	3184

[a] Addition of excess NaOEt. [b] Neat EtOH. [c] Emission wavelength in parentheses. [d] Excitation wavelength in parentheses.

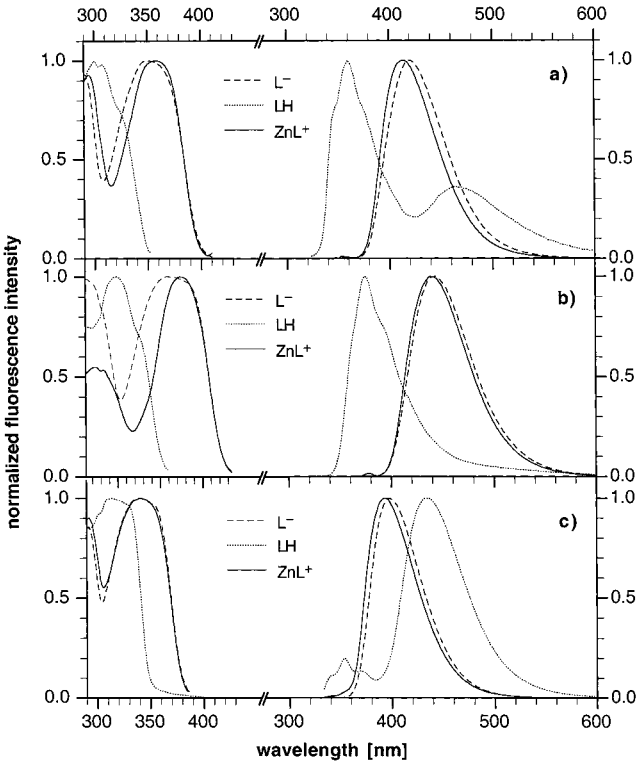

Figure 4. Normalized fluorescence emission and excitation spectra for a) oxazole **4a**, b) thiazole **6a** and c) imidazole **5a** in ethanol at 25 °C. The traces for the protonated ligands (neutral net charge) were measured in neat ethanol, the spectra of the deprotonated ligand (phenolate anion) were recorded after addition of excess NaOEt. The spectra of the Zn(II) complex were obtained at 5 mM total $Zn(OTf)_2$ for (a) and (c) and 500 mM $Zn(OTf)_2$ for graph (b).

which is in agreement with the presence of two distinctly different species. In ethanol, the largely Stokes-shifted band at 464 nm can be attributed to the ESIPT emission of the keto tautomer (^{1}K*).[33] In aqueous solution, the lower energy band at 417 nm is considerably less Stokes shifted (7564 vs 9895 cm^{-1}), and is presumably not due to the emission of the keto tautomer. The band appears at the same energy as the peak emission of the fully deprotonated ligand under basic conditions (Figure 3a). The excitation spectrum recorded at 417 nm shows a shoulder at 350 nm, which also coincides with the observed excitation maximum of the deprotonated phenolate anion. Hence, these data suggest that the lower-energy emission in aqueous solution can be assigned to fluorescence of the deprotonated phenolate anion. Given the p*K* value of 9.23 for the phenol oxygen, at neutral pH the ground-state equilibrium is essentially dominated by the monoprotonated species LH^- (>99%). Therefore, the phenolate anion must be formed in the excited state via intermolecular proton transfer to the solvent. Similar observations were reported for 2-(2′-hydroxyphenyl)-benzimidazole (HBI) in water or binary solvents.[34,35] The strong ability of water to form hydrogen bonds disrupts the intramolecular H-bond required for the ESIPT process and destabilizes the planar conformation. The experimental results suggest that in buffered neutral aqueous solution the intramolecular proton-transfer process is disrupted in favor of the normal emission of the trans rotamer E_t and the phenolate anion.

The emission and excitation spectra of the benzothiazole ligand **6b** resemble those of the oxazole derivative, but with a bathochromic shift of all maxima by 20 to 30 nm (Figure 3b). At neutral pH in aqueous solution the fluorescence spectrum of the thiazole ligand also shows dual emission with a maximum at 436 nm and a weaker shoulder at higher energy (375 nm). The relative intensity of the two bands is just reversed compared to the oxazole emission (**4b**) under the same conditions. The more intense lower-energy band also matches the peak emission of the deprotonated phenolate anion. The excitation spectrum of this band shows a shoulder at 370 nm, which coincides with the excitation maximum of the phenolate anion. As already observed for the oxazole derivative, the lower-energy band can be assigned to emission of the phenolate anion. The p*K* value of the thiazole derivative **6b** is one order of magnitude lower compared to the oxazole ligand (8.25 vs 9.28), which implies that at neutral pH the phenolate anion is present with approximately 10% abundance. This is consistent with the fact that the fluorescence spectrum of the thiazole derivative **6b** is dominated by the lower-energy emission of the phenolate anion, whereas the normal emission at higher energy is the major component for the oxazole ligand **4b**. Interestingly, the emission spectrum of ester **6a** in ethanol exhibits only a single band at 375 nm, which presumably corresponds to the normal emission of the trans-rotamer E_t (Figure 4b). No significant lower-energy band was observed which could be assigned to emission of the keto-tautomer or the phenolate anion. As already found for the oxazole derivative **4b**, the fluorescence spectrum of the thiazole **6b** in neutral aqueous solution is determined by normal emission of the phenolate anion and the trans-rotamer. The ESIPT process is inhibited due to the formation of strong intermolecular hydrogen bonds with solvent molecules, and emission of the keto-tautomer (K*) was not observed, neither in aqueous solution nor in ethanol.

The fluorescence spectrum of the benzimidazole ligand **5b** is composed of three different emission bands (Figure 3c). The quantum yield was measured to be 25% and is comparable to the reported quantum yield of the unsubstituted 2-(2′-hydroxyphenyl)-benzimidazole (HBI) ligand.[33] In aqueous solution at neutral pH, the spectrum is dominated by the highest energy band at 355 nm, which is presumably due to normal emission of the trans-rotamer E_t. This assignment is consistent with previous studies of HBI in ethanol and water, where a maximum of 350 nm was reported for the emission of the trans-rotamer E_t.[32,34,36] Ligand **6b** not only exhibits the short-wavelength emission, but also two weaker, red-shifted emission bands which appear only as shoulders at 396 and 430 nm. The presence of

TABLE 3: Thermodynamic and Photophysical Data for the Complexation of Benzazole 4b, 5b, and 6b with Zn(II) in Aqueous Solution[a]

data	oxazole (**4b**)	imidazole (**5b**)	thiazole (**6b**)
log$K$[b]	3.93 ± 0.01	4.32 ± 0.01	1.97 ± 0.01
Absorption[c] λ_{max} (nm), ϵ($cm^{-1}M^{-1}$)	347, 25100	332, 23200	366, 24500
Excitation[d] λ_{max} (nm)	350 (411)[e]	340 (393)[e]	364 (442)[e]
Emission[d] λ_{max} (nm)	411 (350)[f]	393 (340)[f]	438 (370)[f]
Stokes Shift (cm^{-1})	4487	4675	4491
Quantum Yield	0.26	0.23	0.07

[a] 0.1 M KNO_3, 25 °C, PIPES 10 mM pH 7.20. [b] Apparent binding constant at pH 7.2. [c] Deconvoluted spectra from UV−vis titration. [d] PIPES 10 mM, pH 7.20, 0.1M KNO_3, 32 μM ligand, 5 mM $Zn(OTf)_2$. [e] Emission wavelength in parentheses. [f] Excitation wavelength in parentheses.

three distinctly different species in the excited-state equilibrium is further supported by the fact that the relative intensity of the three bands depends strongly on the excitation wavelength. With decreasing excitation energy, the intensity of the two lower-energy bands increases. In contrast, the fluorescence spectrum of ester **5a** in ethanol shows only two bands of which the lower-energy emission at 435 nm is considerably stronger. Based on published data, the large Stokes shift of 8395 cm^{-1} of this band is consistent with emission of the keto-tautomer ($^1K^*$), whereas the higher energy band at 353 nm can be assigned to the normal emission of the trans-rotamer ($^1E_t^*$).[32,34,36] The observed lower-energy shoulder at 430 nm in aqueous solution is presumably due to emission of the keto-form, whereas the second shoulder at 396 nm can be assigned to the emission of the deprotonated phenolate anion. The emission spectrum under basic conditions in buffered aqueous solution or ethanol (pH > 11) shows a maximum at 396 and 393 nm respectively, which confirms this assignment. Consistent with the emission properties of the thiazole and oxazole ligands, the phenolate emission band is observed in aqueous solution but not in ethanol.

As already described for the thiazole and oxazole derivatives, the ability of water to form strong intermolecular hydrogen bonds with the ligand results in stabilization of the two isomers E_t and E_o, which do not undergo ESIPT (Scheme 3). The fluorescence properties of **5b** at neutral pH are therefore mostly determined by the emission of these two species. This observation contrasts with previously reported results for 2-(2′-hydroxyphenyl)-benzimidazole (HBI) in unbuffered water.[34] Under these conditions, the keto-isomer ($^1K^*$) is responsible for the major emission channel, whereas fluorescence of the trans-rotamer ($^1E_t^*$) is substantially weaker. The difference must be ascribed to the presence of PIPES buffer (10 mM) and the 0.1 molar ionic background. Both components would be expected to further stabilize intermolecular hydrogen bonds.

Complexation Studies. The purpose of this study is exploring the fluorescence properties of benzazole ligands with biologically important metals. Under physiological conditions, complexation with transition metal ions such as Zn(II), Fe(II), Cu(II), or Ni(II) leads to a change in both the absorption and emission spectra of the benzazole ligands. No effect was observed for Ca(II), Mg(II), Na(I), or K(I). Since the complexes with the paramagnetic transition metal ions Cu(II), Fe(II), and Ni(II) are nonfluorescent, the binding studies focused exclusively on the investigation of the Zn(II) complexes by means of absorption and steady-state spectroscopy in aqueous solution at neutral pH.

Absorption Spectra. The binding affinities with Zn(II) for all three ligands **4b**, **5b**, and **6b** were determined by UV−vis spectrophotometric titrations in PIPES buffered solution at pH 7.2 and constant ionic strength (0.1 M KNO_3). The ions of the ionic background (potassium nitrate), as well as the triflate anion introduced as counterion of the Zn(II) salt, have a very low affinity to the ligand and Zn(II) respectively, and should therefore not disturb the equilibrium measurements. The UV absorption spectra were recorded for a set of solutions in which the metal concentration was increased stepwise from 0 to 1 mM (oxazole **4b** and imidazole **6b**) or 50 mM in the case of the thiazole **5b**. The spectra were analyzed over the entire wavelength range using a nonlinear least-squares fit algorithm as implemented in the SPECFIT software package.[49,51] For all three ligands a single set of isosbestic points was observed, which suggests a simple complexation equilibrium. Fitting of the titration curves was found to yield acceptable results only for a 1:1 complexation model. Attempts to use 2:1 or 3:1 stoichiometries yielded deconvoluted spectra with negative absorption values, which further supports the presence of a single equilibrium system with 1:1 complex stoichiometry. A compilation of the curve fitting results as well as the photophysical properties of the three Zn(II) complexes is given in Table 3, and the deconvoluted UV−vis spectra are included in Figure 1. All tabulated binding affinities were measured in buffered solution at constant pH and ionic strength, and therefore correspond to apparent stability constants (logK') under these specific conditions. For all ligands, the lowest energy absorption of the Zn(II) complex shows the typical features of organic chromophores with a broad, structureless band and high extinction coefficient (> 20′000 $M^{-1}cm^{-1}$), which indicates a ligand-centered $\pi\pi^*$ electronic transition. Compared to the monoprotonated, uncomplexed ligands, the absorption maxima are considerably red-shifted, and essentially overlap with the lowest energy band of the corresponding phenolate anion (Figure 1). This similarity suggests that coordination of the metal ion is accompanied by deprotonation of the phenol oxygen, which also acts as donor atom in the Zn(II) complex. The imidazole ligand **5b** has the highest affinity for Zn(II) with log$K$ = 4.32. As would be expected from the smaller π-donor strength of oxygen compared to nitrogen, the oxazole derivative **4b** exhibits a slightly lower affinity with log$K$ = 3.93. Following the same trend, the thiazole ligand, **6b**, binds Zn(II) considerably less tightly with log$K$ = 1.97. The differences in affinity are best visualized in a species distribution plot showing the relative abundance of the complex as a function of total Zn(II) present (Figure 5). The graph illustrates that the oxazole and imidazole derivatives both reach Zn(II) saturation at concentrations around 5 mM, whereas the thiazole ligand **5b** requires a metal concentration of 0.5 M.

Fluorescence Spectra. Using identical conditions as described for the UV−vis binding studies, fluorescence titrations with Zn(II) were performed in aqueous solution for each of the ligands **4b**, **5b**, and **6b**. The 1:1 zinc-complex of oxazole **4b** revealed a more than 50-fold increase in fluorescence intensity compared to the unbound ligand (Figure 6a). A quantum yield of 27% was obtained at Zn(II) saturation, which is nine times greater than the quantum yield of the free ligand under identical conditions. Coordination of Zn(II) appears to inhibit major nonradiative decay pathways leading to an electronically different lowest excited singlet state. Not only are the relative energies of neighboring singlet nπ^* or triplet states expected

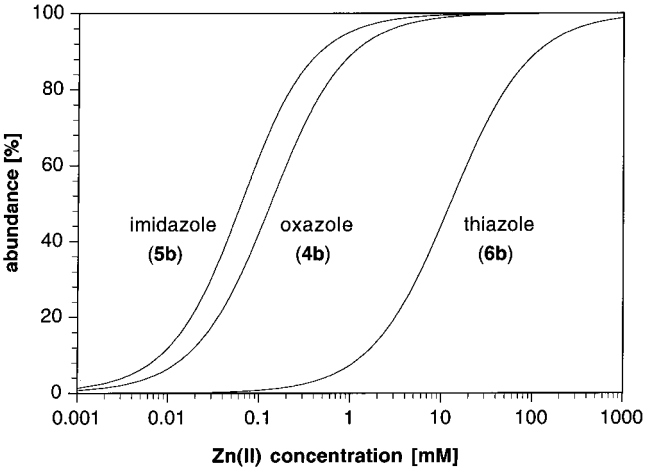

Figure 5. Calculated species distribution diagram as a function of the total Zn(II) concentration for oxazole **4b**, imidazole **5b**, and thiazole **6b** in aqueous solution at pH 7.20 and 25 °C (30 μM total ligand concentration).

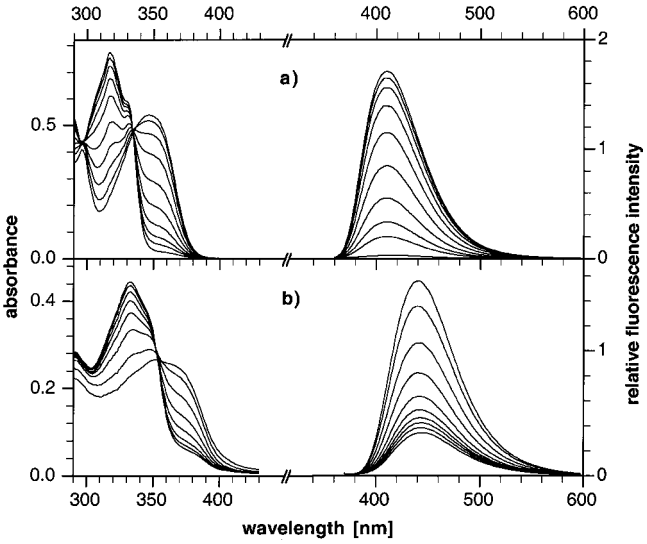

Figure 6. a) Left: UV−vis absorbance of oxazole **4b** as a function of added Zn(II) in 10 mM PIPES at 25 °C. Right: fluorescence emission spectra under identical conditions, excitation at 350 nm. b) Left: UV−vis absorbance of thiazole **6b** as a function of added Zn(II) in 10 mM PIPES at 25 °C. Right: fluorescence emission spectra under identical conditions, excitation at 364 nm.

to be altered, but Zn(II) coordination rigidifies the ligand backbone and prevents nonradiative deactivation through torsional motions of the two aryl moieties. The emission maximum was observed at 411 nm, which is only slightly blue-shifted compared to the emission of the deprotonated phenolate anion. As already discussed in the previous paragraph, the photophysical properties of the Zn(II)-bound ligand are very similar compared to the deprotonated phenolate anion. The excitation spectrum recorded at 411 nm matches the spectrum of the phenolate anion very closely, with almost identical maxima at 350 and 347 nm, respectively. The dramatic increase in fluorescence intensity upon Zn(II) binding prompted us to further explore the suitability of oxazole ligand **4b** as a Zn(II) specific fluorescence probe. Indeed, titration with Fe(II), Cu(II), Ca(II), and Mg(II) did not show any increase in fluorescence intensity, even at high metal concentrations (Figure 8).[56] The titration of thiazole derivative **5b** with Zn(II) showed qualitatively the same result as observed for oxazole **4b**, but the fluorescence intensity increases only about four times compared

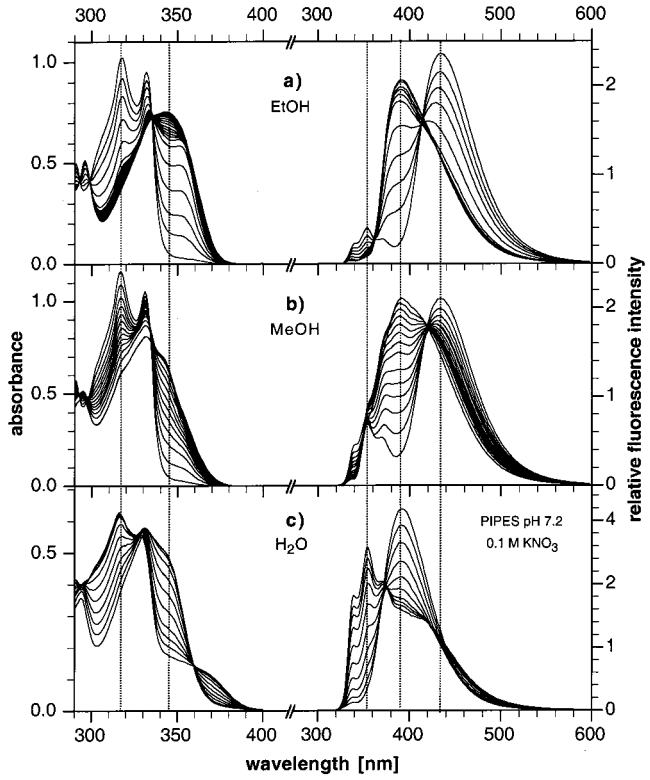

Figure 7. UV-vis absorbance (left) and fluorescence emission spectra (right) of imidazole ligand **5** as a function of added Zn(II) (excitation at the isosbestic point of the UV titration). a) Titration of **5a** in ethanol b) Titration of **5a** in methanol c) Titration of **5b** in aqueous solution (pH 7.20, 10 mM PIPES, 0.1 M KNO_3).

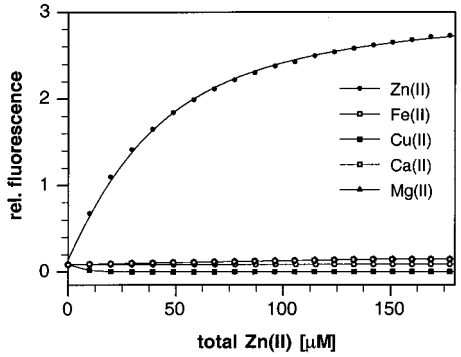

Figure 8. Relative fluorescence intensity (at 411 nm) of ligand **4b** in aqueous solution as a function of various metal cations (pH 7.20, 10 mM PIPES, 0.1 M KNO_3).

to the unbound ligand (Figure 6b). The peak emission appears red-shifted at 438 nm, and is again close to the maximum of 446 nm measured for the phenolate anion.

The fluorescence quantum yields of the oxazole and thiazole derivatives vary significantly between the unbound and Zn(II)-saturated form. In contrast, the imidazole dervative **5b** is strongly fluorescent in the presence and absence of Zn(II). Conclusively, this ligand is the only derivative which would be suitable for the development of ratiometric probes as dicussed in the introductory paragraph. The formation of the keto-tautomer by ESIPT is largely inhibited under physiological conditions, presumably due to the ionic background and buffer used. To explore the influence of metal coordination on the ESIPT process in more detail, we performed Zn(II) titrations not only in aqueous solution, but also in methanol and ethanol using the ester derivative **5a** (Figure 7). As previously shown, in ethanol the ESIPT process yielded strong emission of the keto-tautomer

(^{1}K*). Addition of increasing amounts of Zn(II) revealed a substantial blue-shift in the peak emission from 435 to 393 nm. The keto-tautomer emission as well as the normal emission band of the trans-rotamer (^1E_t*) at higher energy disappeared completely upon saturation with excess Zn(II). Clearly, the intramolecular hydrogen bond has been replaced by coordination to the metal cation, resulting in inhibition of the ESIPT process. Interestingly, the UV−vis spectra measured for an equivalent set of solutions suggest formation of the Zn(II) complex with 2:1 stoichiometry. After addition of 0.5 molar equivalents of Zn(II), the spectral changes became much smaller and a large excess of Zn(II) was required to further affect the absorption spectrum and shift the equilibrium toward the 1:1 complex. Since the titration in ethanol was performed in unbuffered solution, coordination of Zn(II) lowers the pH and therefore complicates the equilibrium system throughout the titration. It is therefore not surprising that nonlinear least-squares analysis of the UV−vis traces using 1:1 and 2:1 complex models was not successful. An identical fluorescence titration in methanol yielded qualitatively the same result. Most importantly, the maxima of the observed emission bands did not shift and therefore allow a direct comparison with the titration carried out in ethanol. The higher polarity and stronger hydrogen-bonding ability of methanol further destabilizes the intramolecular hydrogen bond required for ESIPT. As a result the normal emission of the trans-rotamer, ^1E_t* is significantly increased relative to the keto-emission. Addition of Zn(II) again leads to displacement of the intramolecular hydrogen bond by the metal cation and yields an emission band virtually identical to the one observed in ethanol. A qualitative analysis of the corresponding UV−vis titration in methanol reveals a single set of isosbestic points with no indication for the formation of a 2:1 complex. The greater polarity of methanol apparently stabilizes the positively charged 1:1 complex, whereas in ethanol the equilibrium is more in favor of the neutral 2:1 species. Finally, an analogous titration was performed with acid derivative **5b** in aqueous solution at neutral pH. As already pointed out previously, the fluorescence spectrum of **5b** is dominated by the normal emission of the trans-rotamer, whereas the lower energy keto-tautomer emission band appears only as a shoulder (Figure 7c). Addition of Zn(II) again generated a single emission band with a maximum at 393 nm, which overlaps with the maxima observed in ethanol and methanol. Nonlinear least-squares fit analysis of the UV−vis traces for an identical titration are in agreement with a 1:1 complex stoichiometry, which is additionally supported by the presence of a single set of isosbestic points. In the presence of excess Zn(II), both emission and excitation spectra were independent of the excitation or emission wavelength at which the spectra were recorded, an observation which is consistent with the formation of a single species (1:1 complex).

Conclusions

Numerous studies focused on the characterization of intramolecular excited-state proton transfer of 2-(2′-hydroxyphenyl)-benzazoles in nonpolar and polar solvents, but only few investigations were carried out in aqueous solution, and none of them under physiological conditions in the presence of 0.1 M ionic background. The low solubility of 2-(2′-hydroxyphenyl)benzazoles in water, particularly in the presence of additional ionic background, hampers photophysical studies under these conditions. To overcome these limitations, we synthesized a series of derivatives, which are well soluble at neutral pH due to the presence of a negatively charged carboxylate group. Under physiological conditions, the fluorescence properties of all three derivatives **4**, **5**, and **6**, differ substantially with respect to previously published results in nonaqueous solvents. Most important, in all cases the ESIPT process is disrupted, presumably due to intermolecular hydrogen bonding with surrounding water molecules and increased stabilization of the trans-rotamer E_t, which cannot undergo the ESIPT process. Titration of the oxazole derivative **4b** with Zn(II) at neutral pH revealed a strong increase in the fluorescence. The response is specific for Zn(II) and was not observed for other biologically important metals such as Fe(II), Cu(II), Mg(II), or Ca(II). With a log$K$ of 3.93 (corresponding to the dissociation constant $K_d = 117\ \mu$M), oxazole **4b** would be suitable as a fluorescence probe in a biological environment to gauge Zn(II) concentrations in the range from 10 μM to 1 mM. The thiazole derivative **6b** shows qualitatively a similar behavior, but with substantially lower binding affinity and lower quantum yield. In contrast, the imidazole derivative **5b** revealed a slightly higher affinity for Zn(II) with a log$K$ of 4.32 ($K_d = 47\ \mu$M). Furthermore, the titration in ethanol, methanol, and buffered aqueous solution showed that inhibition of ESIPT via metal coordination is a promising concept for the development of fluorescence probes with ratiometric emission properties. The changes of the fluorescence intensity ratio at two selected wavelengths going from the unbound ligand to its metal-saturated form, determine the dynamic resolution of the probe and is therefore of great importance.[2] Typically, with increasing shift of the peak emission the overall change of emission ratios is also increasing, which generally improves the dynamic resolution. Inhibition of ESIPT via metal coordination as demonstrated by titration of **5a** with Zn(II) in ethanol shows a significant wavelength shift, together with a substantial ratio increase by a factor of 13.7. For biological applications, the solvent polarity dependence of the emission spectrum is a limiting factor, and might lead to artifacts due to partitioning of the probe into vesicular membranes. Future research will concentrate on the identification of ESIPT molecules which do not allow rotational isomerism in the groundstate, and therefore eliminate the polarity dependent normal emission observed for 2-(2′-hydroxyphenyl)benzazole derivatives.

Acknowledgment. Financial support via startup funds from the Georgia Institute of Technology is gratefully acknowledged. We also thank S. Shealy and D. Bostwick for mass spectral data, C. Burda (Case Western Reserve University, Cleveland) for valuable discussions, and L. Lawson and B. Ayres for a critical review of the manuscript.

References and Notes

(1) DeSilva, A. P.; Gunaratne, H. Q. N.; Gunnlaugsson, T.; Huxley, A. J. M.; McCoy, C. P.; Rademacher, J. T.; Rice, T. E. *Chem. Rev.* **1997**, *97*, 1515.

(2) Grynkiewicz, G.; Poenie, M.; Tsien, R. Y. *J. Biol. Chem.* **1985**, *260*, 3440.

(3) Haugland, R. P. *Handbook of Fluorescent Probes and Research Chemicals*; Molecular Probes, Inc.: Eugene, OR, 1996.

(4) Chou, P. T.; Martinez, M. L.; Clements, J. H. *Chem. Phys. Lett.* **1993**, *204*, 395.

(5) Parthenopoulos, D. A.; McMorrow, D.; Kasha, M. *J. Phys. Chem.* **1991**, *95*, 2668.

(6) Chou, P. T.; Martinez, M. L. *Radiat. Phys. Chem.* **1993**, *41*, 373.

(7) Sytnik, A.; Kasha, M. *Rad. Phys. Chem.* **1993**, *41*, 331.

(8) Renschler, C. L.; Harrah, L. A. *Nucl. Instrum. Methods Phys. Res., Sect. A* **1985**, *A235*, 41.

(9) O'Connor, D. B.; Scott, G. W.; Coulter, D. R.; Yavrouian, A. *J. Phys. Chem.* **1991**, *95*, 10252.

(10) Keck, J.; Kramer, H. E. A.; Port, H.; Hirsch, T.; Fischer, P.; Rytz, G. *J. Phys. Chem.* **1996**, *100*, 14468.

(11) Sytnik, A.; Delvalle, J. C. *J. Phys. Chem.* **1995**, *99*, 13028.

(12) Sytnik, A.; Kasha, M. *Proc. Natl. Acad. Sci. U.S.A.* **1994**, *91*, 8627.
(13) Sytnik, A.; Gormin, D.; Kasha, M. *Proc. Natl. Acad. Sci. U.S.A.* **1994**, *91*, 11968.
(14) Barbara, P. F.; Walsh, P. K.; Brus, L. E. *J. Phys. Chem.* **1989**, *93*, 29.
(15) Laermer, F.; Elsaesser, T.; Kaiser, W. *Chem. Phys. Lett.* **1988**, *148*, 119.
(16) Arthen-Engeland, T.; Bultmann, T.; Ernsting, N. P.; Rodriguez, M. A.; Thiel, W. *Chem. Phys.* **1992**, *163*, 43.
(17) Douhal, A.; Fiebig, T.; Chachisvilis, M.; Zewail, A. H. *J. Phys. Chem. A* **1998**, *102*, 1657.
(18) Marks, D.; Prosposito, P.; Zhang, H.; Glasbeek, M. *Chem. Phys. Lett.* **1998**, *289*, 535.
(19) Nagaoka, S.; Nagashima, U.; Ohta, N.; Fujita, M.; Takemura, T. *J. Phys. Chem.* **1988**, *92*, 166.
(20) Frey, W.; Elsaesser, T. *Chem. Phys. Lett.* **1992**, *189*, 565.
(21) Frey, W.; Laermer, F.; Elsaesser, T. *J. Phys. Chem.* **1991**, *95*, 10391.
(22) Lochbrunner, S.; Schultz, T.; Schmitt, M.; Shaffer, J. P.; Zgierski, M. Z.; Stolow, A. *J. Chem. Phys.* **2001**, *114*, 2519.
(23) Lochbrunner, S.; Wurzer, A. J.; Riedle, E. *J. Chem. Phys.* **2000**, *112*, 10699.
(24) Ernsting, N. P.; Kovalenko, S. A.; Senyushkina, T.; Saam, J.; Farztdinov, V. *J. Phys. Chem. A* **2001**, *105*, 3443.
(25) Nagaoka, S.; Kusunoki, J.; Fujibuchi, T.; Hatakenaka, S.; Mukai, K.; Nagashima, U. *J. Photochem. Photobiol. A* **1999**, *122*, 151.
(26) Elsaesser, T.; Schmetzer, B. *Chem. Phys. Lett.* **1987**, *140*, 293.
(27) Krishnamurthy, M.; Dogra, S. K. *J. Photochem.* **1986**, *32*, 235.
(28) Wang, X. F.; Herman, B. In *Fluorescence Imaging Spectroscopy and Microscopy*; Winefordner, J. D., Ed.; John Wiley & Sons: New York, 1996; Vol. 137.
(29) König, K.; Simon, U.; Halbhuber, K. J. *Cell. Mol. Biol.* **1996**, *42*, 1181.
(30) So, P. T. C.; Dong, C. Y.; Masters, B. R.; Berland, K. M. *Annu. Rev. Biomed. Eng.* **2000**, *2*, 399.
(31) König, K. *J. Microscopy* **2000**, *200*, 83.
(32) Das, K.; Sarkar, N.; Majumdar, D.; Bhattacharyya, K. *Chem. Phys. Lett.* **1992**, *198*, 443.
(33) Das, K.; Sarkar, N.; Ghosh, A. K.; Majumdar, D.; Nath, D. N.; Bhattacharyya, K. *J. Phys. Chem.* **1994**, *98*, 9126.
(34) Mosquera, M.; Penedo, J. C.; Rios Rodríguez, M. C.; Rodríguez-Prieto, F. *J. Phys. Chem.* **1996**, *100*, 5398.
(35) Roberts, E. L.; Dey, J.; Warner, I. M. *J. Phys. Chem. A* **1997**, *101*, 5296.
(36) Sinha, H. K.; Dogra, S. K. *Chem. Phys.* **1986**, *102*, 337.
(37) Grellmann, K. H.; Mordzinski, A.; Heinrich, A. *Chem. Phys.* **1989**, *136*, 201.
(38) Itoh, M.; Fujiwara, Y. *J. Am. Chem. Soc.* **1985**, *107*, 1561.
(39) Nagaoka, S.; Itoh, A.; Mukai, K.; Hoshimoto, E.; Hirota, N. *Chem. Phys. Lett.* **1992**, *192*, 532.
(40) Stephan, J. S.; Grellmann, K. H. *J. Phys. Chem.* **1995**, *99*, 10066.
(41) Tanaka, K.; Deguchi, M.; Yamaguchi, S.; Yamada, K.; Iwata, S. *J. Heterocycl. Chem.* **2001**, *38*, 131.
(42) Elsaesser, T.; Schmetzer, B.; Lipp, M.; Baeuerle, R. J. *Chem. Phys. Lett.* **1988**, *148*, 112.
(43) Potter, C. A. S.; Brown, R. G.; Vollmer, F.; Rettig, W. *J. Chem. Soc., Faraday Trans.* **1994**, *90*, 59.
(44) Brewer, W. E.; Martinez, M. L.; Chou, P. T. *J. Phys. Chem.* **1990**, *94*, 1915.
(45) Shamim, M. T.; Ukena, D.; Padgett, W. L.; Hong, O.; Daly, J. W. *J. Med. Chem.* **1988**, *31*, 613.
(46) Demas, J. N.; Crosby, G. A. *J. Phys. Chem.* **1971**, *75*, 991.
(47) Gran, G. *Analyst (London)* **1951**, *77*, 661.
(48) Gans, P.; O'Sullivan, B. *Talanta* **2000**, *51*, 33.
(49) Binstead, R. A.; Zuberbühler, A. D. *SPECFIT Global Analysis System*; 3.0.27 ed.; Spectrum Software Associates, Marlborough MA 01752, 2001.
(50) Mickelson, J. W.; Jacobsen, E. J.; Carter, D. B.; Im, H. K.; Im, W. B.; Schreur, P.; Sethy, V. H.; Tang, A. H.; McGee, J. E.; Petke, J. D. *J. Med. Chem.* **1996**, *39*, 4654.
(51) Maeder, M.; Zuberbühler, A. D. *Anal. Chem.* **1990**, *62*, 2220.
(52) Durmis, J.; Karvas, M.; Manasek, Z. *Collect. Czech. Chem. Commun.* **1973**, *38*, 215.
(53) Catalan, J.; Claramunt, R. M.; Elguero, J.; Laynez, J.; Menendez, M.; Anvia, F.; Quian, J. H.; Taagepera, M.; Taft, R. W. *J. Am. Chem. Soc.* **1988**, *110*, 4105.
(54) Yang, G.; Morlet-Savary, F.; Peng, Z.; Wu, S.; Fouassier, J.-P. *Chem. Phys. Lett.* **1996**, *256*, 536.
(55) Mordzinski, A.; Grellmann, K. H. *J. Phys. Chem.* **1986**, *90*, 5503.
(56) Similar results were reported very recently for 2-(3,5,6-trifluoro-2-hydroxy-4-methoxyphenyl)benzoxazole in organic and mixed aqueous solvents: Tanaka, K.; Kumagai, T.; Aoki, H.; Deguchi, M.; Iwata, S. *J. Org. Chem.* **2001**, *66*, 7328.